ELSEVIER

Chemical Engineering Science 62 (2007) 1636–1649

Chemical Engineering Science

www.elsevier.com/locate/ces

Modeling of a SOFC fuelled by methane: From direct internal reforming to gradual internal reforming

J.-M. Klein[a,*], Y. Bultel[a], S. Georges[a], M. Pons[b]

[a]*Laboratoire d'Electrochimie et de Physico-Chimie des Matériaux et des Interfaces (LEPMI), UMR 5631 CNRS-INPG-UJF, ENSEEG, BP 75, 38402 Saint Martin d'Hères, France*

[b]*Laboratoire de Thermodynamique et de Physicochimie Métallurgique (LTPCM), UMR 5614 CNRS-INPG-UJF, ENSEEG, BP 75, 38402 Saint Martin d'Hères, France*

Received 27 July 2006; received in revised form 13 November 2006; accepted 17 November 2006
Available online 24 November 2006

Abstract

Natural gas appears to be a fuel of great interest for SOFC systems. The principal component of natural gas is methane, which can be converted into hydrogen by direct or gradual internal reforming (DIR or GIR) within the SOFC anode. However, DIR requires a large amount of steam to produce hydrogen. If the injected mixture contains very small quantities of steam, GIR is then obtained. With GIR, the risk of carbon formation is even greater. This paper proposes a model and simulation, using the CFD-Ace software package, of the behaviour of a tubular SOFC using GIR and a comparison between utilization in DIR and GIR. A thermal study is included in the model and a detailed thermodynamic analysis is carried out to predict the carbon formation boundary for SOFCs fuelled by methane. Thermodynamic equilibrium calculations taking into account Boudouard and methane cracking reactions allowed us to investigate the occurrence of carbon formation. Simulations were used to calculate the distributions of partial pressures for all the gas species (CH_4, H_2, CO, CO_2, H_2O), current densities and potentials in both electronic and ionic phases within the anode part (i.e., gas channel and cermet anode). The simulations indicate that there is no decrease in electrochemical performance if GIR is used rather than DIR. A thermal study appears to confirm that the cooling effect due to the endothermic reforming reaction is eliminated in GIR, but the thermodynamic study indicates that carbon formation can be suspected for x_{H_2O}/x_{CH_4} ratios lower than one.

Keywords: SOFC; Modeling; Simulation; CFD Ace; Gradual internal reforming

1. Introduction

Given the increasing and irreversible consumption of fossil fuels, there is now an urgent need for a transition to renewable energy sources. With this aim in mind, fuel cells appear to offer an interesting alternative solution as power generators. Fuel cells directly convert chemical energy into electric power, with high energetic efficiency and low pollution levels from the exhaust gases.

SOFCs (solid oxide fuel cells) are promising candidates for generating power while preserving the environment. Nowadays most SOFC developers use a fuel containing a significant proportion of hydrogen. However, the high operating temperature (973–1273 K) of SOFCs allows considerable flexibility in terms of feed fuels (fossil fuel, natural gas, methanol, ethanol and particularly biogas that contains methane) and the most interesting fuel for SOFC systems remains methane. It is clear that the DIR operating conditions pose many problems. Indeed the steam addition will involve a reduction in the open circuit voltage. Moreover, the cooling effect due to the endothermic reaction can engage thermal stress into the ceramic anode which can lead to the anode destruction. Finally, the problem of carbon deposition is not still resolved. Nevertheless, nowadays natural gas is directly available whereas hydrogen must be produced and thus DIR is a very hopeful method. Indeed, gradual internal reforming (GIR) (Vernoux et al., 1998) or direct internal reforming (DIR) within the SOFC anode (Ahmed and Foger,

* Corresponding author. Tel.: +33 4 76 82 65 70; fax: +33 4 76 82 67 77.
E-mail address: jean-marie.klein@lepmi.inpg.fr (J.-M. Klein).

0009-2509/$ - see front matter © 2006 Elsevier Ltd. All rights reserved.
doi:10.1016/j.ces.2006.11.034

2000; Vernoux et al., 2000) allow the conversion of methane into hydrogen without using a separate reformer. Such a concept is convenient for high-temperature fuel cells in which the steam reforming reaction can be sustained with catalysts. The reforming reaction at the anode and the water gas shift reaction are carried out over a supported catalyst such as nickel. These reactions provide the system with the dihydrogen required by the electrochemical reaction. SOFC internal reforming is thus designed by closely coupling the catalytic reforming reaction and the electrochemical oxidation reaction within the anodic side of the cell.

Recent literature provides evidence of significant research and development efforts focused on DIR modeling within the SOFC anode. Lehnert et al. (2000) proposed one-dimensional simulations based on a geometry integrating an anode supported by a planar substrate and taking into account mass transport. Multi-component transport was described using the mean transport pore model (MTPM), based on three microstructure parameters (porosity, tortuosity and mean pore radii). Special attention was paid by Suwanwarangkul et al. (2003) to describing concentration polarization with different models (Fick's law, dusty-gas and Stefan–Maxwell models) for a $H_2/H_2O/CO/CO_2$ mixture. The MTPM model was extended by Ackmann et al. (2003) into a two-dimensional thermal approach including electrochemical and chemical reactions as heat sources. Some more recent studies offer models of SOFCs from a detailed electrochemical analysis and a fluid-dynamic calculation of internal heat transfer conditions using a finite volume method (Morel et al., 2005; Larrain et al., 2003; Campanari and Iora, 2004). Finally, some general models have been developed, taking into account velocity fields of air and fuel flows, heat generation by ohmic and thermodynamic effects and convective heat-transfer. Other studies have focused on the mass transfer of active chemical species, including electrochemical processes and the distribution of electric potential within electrodes and electrolyte (Aguiar et al., 2004; Li and Suzuki, 2004). All these studies assumed that steam reforming and water gas shift reactions take place within the porous anode, whereas electrochemical oxidation of hydrogen and carbon monoxide occurs close to the electrolyte/anode interface.

GIR, like DIR, is based on local coupling between steam reforming of the fuel, which occurs on a catalyst (Nickel), and electrochemical oxidation of hydrogen, which occurs at the electrode triple-phase perimeter. GIR also enables the hydrogen required by the electrochemical reaction to be generated in situ. However, unlike DIR, which requires large amounts of steam, this process requires very small quantities of steam at the fuel inlet. In fact, the steam used by the reforming reaction is generated by the electrochemical reaction all along the cell. This approach is based on work by Vernoux et al. (1998) and Georges et al. (2006) who have studied the feasibility of GIR working in SOFCs.

The present study proposes a model of a SOFC including a gas diffusion electrode model to simulate the behaviour of a tubular SOFC using the CFD-Ace software package. A realistic triple phase boundary distribution is considered through the porous electrode thickness. The electrochemical reactions within the porous electrodes are described using the Butler–Volmer equations at the triple phase boundary. This gas diffusion electrode model can be compared to some studies on MCFC porous electrode modeling (Yuh and Selman, 1992; Fontes et al., 1997). In particular, this approach is very close to the three-phase homogeneous model developed by Prins-Jansen et al. (1996). However, on the anodic side, we have included reforming and water gas shift reactions, which occur in parallel with hydrogen oxidation. Modeling is based on solving conservation equations off mass, momentum, energy, species and electric current by using a finite volume approach on two-dimensions grids of arbitrary topology. Simulations with the CFD-Ace software package allow the calculation of the distributions of partial pressures (CH_4, H_2, CO, CO_2, and H_2O), current density and potentials of electronic and ionic phases within the anode part (i.e., gas channel and cermet anode), and finally the calculation of the thermal gradient in the cell.

Based on previous approaches described by Hou and Hughes (2001), a detailed thermodynamic analysis taking into account the Boudouard reaction and methane cracking reactions is carried out to predict the carbon formation boundary for SOFCs fuelled by methane. The formation of carbon predicted by thermodynamic equilibrium calculations is then discussed from the values of the driving forces for carbon deposition. It is worth mentioning that this driving force for carbon deposition is only the indicator of carbon presence in the system and does not provide any information about the amount of carbon and its deposition rate. This approach is used to investigate the GIR process. Indeed, carbon deposition, due to the depletion of steam along the cell, seems to be the major limitation of GIR operation.

In this study, the H_2O/CH_4 ratio and current densities are varied in order to identify a suitable region for SOFC operation which does not suffer from carbon formation.

2. Tubular SOFC model

2.1. Description of the tubular SOFC

A tubular SOFC is a cylindrical assembly of an electrolyte sandwiched between an anode and a cathode. The oxidant gas is introduced through a central injection tube, and the fuel gas is supplied to the exterior of the tube. In this arrangement, the fuel gas flows past the anode on the exterior of the cell in parallel to the oxidant gas (co-flow). The tube length for modeling is 30 mm and therefore only the inlet of the cell is taken into account in the model. The thicknesses of the different parts of the tubular SOFC are given in Table 1. The geometry used in

Table 1
Geometric parameters of the tubular SOFC

Geometry	Thickness (mm)
Cathode	0.10
Electrolyte	1.00
Anode	0.20
Collector (×2)	0.10
Gas channel (×2)	3.00

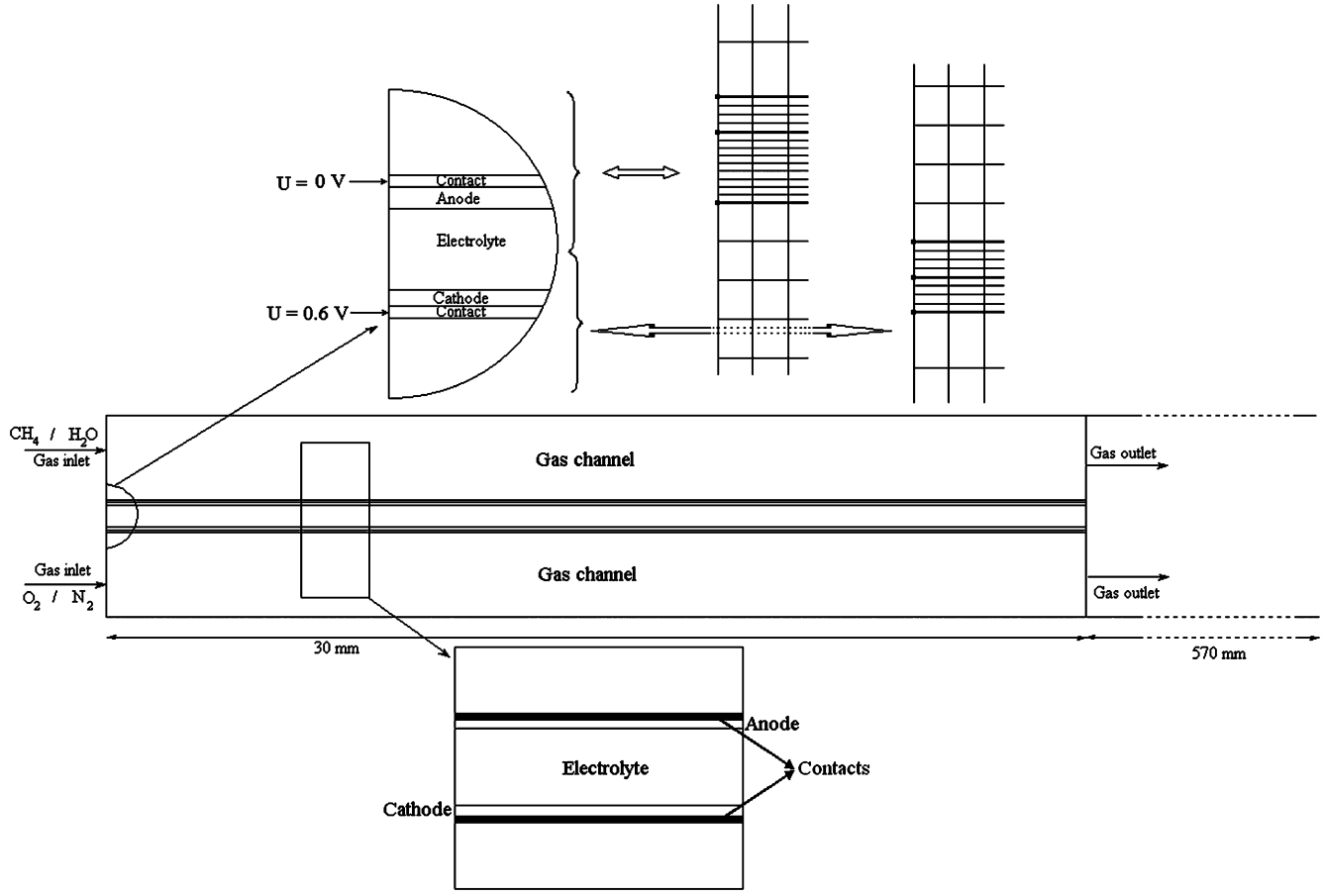

Fig. 1. Geometry of the tubular SOFC cell.

this model is an electrolyte-supported geometry. This choice was made to take into account the original set-up designed to demonstrate the GIR in the SOFC and used by Georges et al. (2006) in their experimental study.

In the present model, mass and charge transport phenomena coupled with chemical and electrochemical reactions are investigated within the inlet of a tubular SOFC as depicted in Fig. 1. A finite volume method using a computational grid (Mazumder and Cole, 2003) is used to solve mass, charge, energy, momentum balances including transport through porous media, and chemical and electrochemical reactions within the porous electrodes in a gas diffusion electrode model. The set of resulting conservation equations is solved using the commercial software package CFD-Ace (ESI group, 2006). This model deals with two-dimensional geometry in steady state conditions.

The O_2/N_2 and CH_4/H_2O mixtures are, respectively, supplied at the air cathode and the anode gas channel. The anodic fuel consumption results from both internal reforming and water gas shift reactions. Fuel composition can include any combination of methane and steam: an equimolar mixture of methane and water can be used for operation in DIR; a mixture where the quantity of water is very low can be used to approach GIR operation.

In the gas phase, the mass conservation equation is described by Mazumder and Cole (2003).

The conservation equations for the transport of N species in a porous media have already been described by Klein et al. (in press), when compressibility and turbulence effects are not taken into account.

The conservation equation for energy (Eq. (1)) may be written as (Mazumder and Cole, 2003)

$$\frac{\partial}{\partial t}\left[(1-\varepsilon)\rho_B h_B + \varepsilon\rho h\right] + \nabla.(\varepsilon\rho\mathbf{v}h) = \nabla.\mathbf{q} + \varepsilon\boldsymbol{\delta}.\nabla\mathbf{v} + \varepsilon\frac{\mathrm{d}p}{\mathrm{d}t} - j_t\left(\frac{S}{V}\right)_{\mathrm{eff}}\eta + \frac{|\mathbf{i}.\mathbf{i}|}{\sigma}, \quad (1)$$

where h is the gas mixture enthalpy, ρ is the mixture density, $\mathbf{v}$ is the velocity vector of the gas mixture and ε is the porosity. Finally, p is the pressure, $\boldsymbol{\delta}$ is the shear stress tensor and h_B and ρ_B are, respectively, the solid phase enthalpy and density. The heat flux, $\mathbf{q}$, is comprised of contributions due to thermal conduction and species diffusion (Eq. (2)) and is written as

$$\mathbf{q} = \lambda\nabla T + \sum_i \mathbf{J}_i h_i, \quad (2)$$

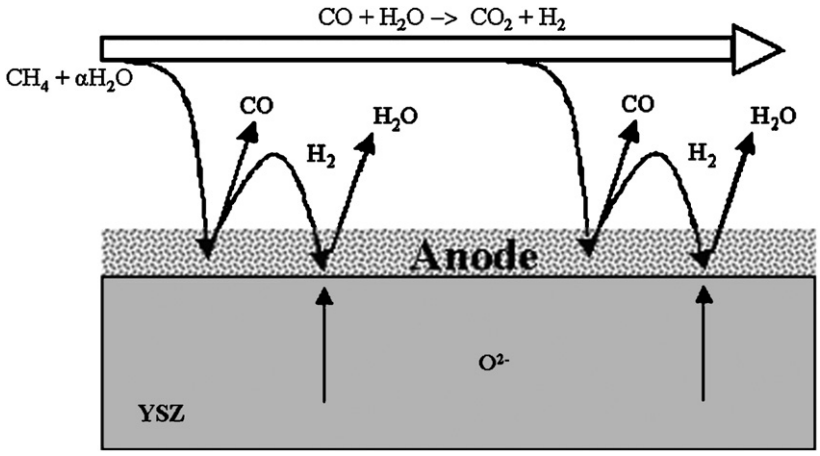

Fig. 2. DIR or GIR of methane by steam.

h_i being species i enthalpies (defined here as the sum of the enthalpy of formation and the sensitive enthalpy), $\mathbf{J}_i$ their diffusion fluxes, and T the temperature. The thermal conductivity, λ, of the porous medium is an effective thermal conductivity of the fluid and solid regions in combination (Eq. (3)) and may be written as

$$\lambda = -2\lambda_B + \frac{1}{(\varepsilon/2\lambda_B + \lambda_F) + ((1-\varepsilon)/3\lambda_B)}, \tag{3}$$

where λ_B and λ_F are the thermal conductivities of the solid and fluid regions, respectively. The last two terms in Eq. (1) represent electrical work and Joule heating, respectively. The irreversible losses due to reactions (conversion of chemical energy to heat energy) manifest themselves automatically through the second term on the right-hand side of Eq. (2) because the definition of enthalpy includes both the enthalpy of formation and the sensitive enthalpy.

Mass and charge balances are numerically solved with regard to the following boundary conditions. Potentials are set to zero for the anodic collector and to an input value for the cathodic one. Ionic current is assumed to be zero on the surface of both collectors but variable elsewhere.

Finally, gas transport within the porous electrode is described by using the combination of diffusive transport (Stefan–Maxwell and Knudsen diffusions) and convective transport.

2.2. Anode

The anode material is a nickel and yttrium stabilized zirconia cermet (Ni-YSZ). The anode is considered for modeling purposes as a porous gas diffusion electrode wherein the electrochemical reaction occurs at the triple phase boundary, i.e., at the interface between the electronic conductor (nickel), ionic conductor (YSZ) and gas phase. Current density is thus the sum of two quite distinct contributions: one related to ionic species and the other to electron transport. Mass transport occurs within the gas pores and charge transport phenomena depend on four electric parameters: ionic and electronic conductivities σ_{aS}, σ_{aM} ($\Omega^{-1}\,\mathrm{m}^{-1}$) and potentials ϕ_{aS} and ϕ_{aM} (V).

DIR(and also GIR) involves adding the reforming function to the SOFC anode (Fig. 2) (Vernoux et al., 1998), a direct production of hydrogen from methane being possible due to the high temperature in the fuel cell.

Methane can thus be converted into H_2 and CO through the steam reforming reaction (Eq. (4)) and the water gas shift (Eq. (5))

$$CH_4 + H_2O \leftrightarrow CO + 3H_2, \tag{4}$$

$$CO + H_2O \leftrightarrow CO_2 + H_2 \tag{5}$$

while hydrogen is electrochemically oxidized within the anode (Eq. (6)):

$$\tfrac{1}{2}\,H_2 + \tfrac{1}{2}\,O^{2-} \rightarrow \tfrac{1}{2}\,H_2O + e^-. \tag{6}$$

The catalytic steam reforming reaction (Eq. (4)) occurs at the surface of the nickel catalyst with a reaction rate (Eq. (7)) ($\mathrm{kmol\,m^{-2}\,s^{-1}}$) described by the Arrhenius law (Lehnert et al., 2000; Hou and Hughes, 2001)

$$r_{E1} = 63.6 \times T^2 \times \exp\left(-\frac{27\,063}{T}\right)[CH_4][H_2O] - 3.7 \times 10^{-14} \times T^4 \times \exp\left(-\frac{232.78}{T}\right)[CO][H_2]^3, \tag{7}$$

where $[i]$ is the concentration of gas species i ($\mathrm{kmol\,m^{-3}}$) and T temperature (K).

Unlike the reforming reaction (Eq. (4)), the shift reaction (Eq. (5)) occurs wherever the gas is present, either in the gas channel or in the pores. Its reaction rate ($\mathrm{kmol\,m^{-3}\,s^{-1}}$) can be expressed on the basis of literature data (Lehnert et al., 2000;

Hou and Hughes, 2001) as (Eq. (8))

$$r_{E2} = 1199 \times T^2 \times \exp\left(-\frac{12\,509}{T}\right)[\mathrm{CO}][\mathrm{H_2O}] - 6.77 \times 10^4 \times T^2 \times \exp\left(-\frac{16\,909}{T}\right)[\mathrm{CO_2}][\mathrm{H_2}]. \quad (8)$$

Finally, the kinetics of the electrochemical reaction (Eq. (6)) within the porous electrode can be described using the Butler–Volmer equation at the triple phase boundary (Eq. (9))

$$j_{at} = j_{a0}\left(\exp\left(\frac{\alpha_a F}{RT}\eta_a\right)\frac{[\mathrm{H_2}]}{[\mathrm{H_2}]_0} - \exp\left(-\frac{\alpha_c F}{RT}\eta_a\right)\right). \quad (9)$$

Here the Faradic current density is expressed in $\mathrm{A\,m^{-2}}$. The overpotential η (Eq. (10)) is defined as the difference between electronic (ϕ_{aM}) and ionic (ϕ_{aS}) potential as

$$\eta_a = \phi_{aM} - \phi_{aS} - E_{a0} \quad (10)$$

and is locally determined within the porous electrode by separately solving the equations related to electronic and ionic potentials. E_{a0} is the potential difference between the electrolyte and the nickel at equilibrium, i.e. when no current is flowing.

The other parameters are: the symmetry factors α_a and α_c determined from the experimental Tafel slopes, the exchange current density j_{a0} ($\mathrm{A\,m^{-2}}$), the Faraday constant F and the ideal gas law constant R. $[\mathrm{H_2}]$ is the interfacial concentration while $[\mathrm{H_2}]_0$ refers to concentration values at the reference state at which the reference current density is prescribed.

The current in a porous electrode can be split into two parts: one part flowing through the electrolyte phase and the other through the electronic phase of the porous matrix. During electrochemical reactions, electrons are then transferred from the ionic phase to the electronic phase, or vice versa. If we consider an electrochemical reaction occurring at the anode, charge conservation may thus be expressed from Ohm's law (Eq. (11)) as

$$\nabla.(\sigma_{aS}\nabla\Phi_{aS}) = -\nabla.(\sigma_{aM}\nabla\Phi_{aM}) = j_{at}\left(\frac{S}{V}\right)_{\mathrm{eff}}. \quad (11)$$

Mass balances for each gas phase species i have already been detailed in a previous study by Klein et al. (in press).

For the description of the diffusion term taken into account in the mass balances, the diffusion flux is given by (Eq. (12))

$$\mathbf{J}_i = \rho D_{i,\mathrm{eff}}\nabla w_i + \frac{\rho w_i}{M} D_{i,\mathrm{eff}}\nabla M - \rho w_i \sum_j D_{j,\mathrm{eff}}\nabla w_j - \rho w_i \frac{\nabla M}{M}\sum_j D_{j,\mathrm{eff}} w_j \quad (12)$$

depending on the mass fraction of species i (w_i), the mass fraction of all the other components of the mixture (w_j) and the molar mass of the gas mixture (M).

The effective mass diffusion coefficient $D_{i,\mathrm{eff}}$ is used to take into account the porous medium in the Stefan–Maxwell diffusion (Eq. (12)) relation (Bird et al., 1960), and is to be deduced from the free stream diffusion coefficient D_i by the so-called Bruggemann model (Bruggemann, 1935) depending on tortuosity τ. Simulations were performed here with a tortuosity of 1.5, a classical value from the literature (Springer et al., 1991; Natarajan and Nguyen, 2001) in the absence of more accurate data.

Table 2
Kinetic data for electrochemical reactions

	Anode	Cathode
$(S/V)\,j_0$ ($\mathrm{A\,m^{-3}}$)	10^{11}	10^{10}
α_a	0.7	–
α_c	–	0.7

2.3. Cathode

The cathode is a porous lanthanum manganite ($La_{0.7}Sr_{0.3}MnO_{3-\delta}$) doped with YSZ solid phases. Its behaviour is described in the same way as previously for the anode.

The oxygen reduction reaction occurs at the cathode from the electrochemical reaction (Eq. (13)).

$$\tfrac{1}{4}\,\mathrm{O_2} + \mathrm{e^-} \rightarrow \tfrac{1}{2}\,\mathrm{O^{2-}}. \quad (13)$$

The Faradic current j_{ct} at the cathode is then obtained from a Butler–Volmer equation similar to Eq. (9).

The kinetic data used in the Butler–Volmer equations (exchange current density j_0 (Costamagna et al., 2002), symmetry factors α_a and α_c) are listed in Table 2 for both anode and cathode.

2.4. Electrolyte

The electrolyte material is YSZ, which is a suitable ionic conductor at high temperatures. Conditions of zero electronic current and zero electronic voltage are imposed in the electrolyte to ensure that the electrolyte is completely impermeable to electron circulation. The electrolyte potential is thus expressed by a classical Ohm's law without any charge creation or consumption within the electrolyte (Eq. (14))

$$\sigma_{eS}\left(\frac{\partial^2\phi_{eS}}{\partial x^2} + \frac{\partial^2\phi_{eS}}{\partial y^2}\right) = 0. \quad (14)$$

2.5. Simulation parameters

Table 3 provides a brief description of the properties (EG&G Services, 2000; Aruna et al., 1998; Hecht et al., 2005; Lee et al., 2002; Ullmann et al., 2000) of the materials currently used in the various cell components of the tubular SOFC at 1173 K. ε is the porosity (ratio of the volume occupied by pores to the total volume of porous solid), κ represents the permeability in $\mathrm{m^2}$, λ_B is the solid phase thermal conductivity in $\mathrm{W\,m^{-1}\,K^{-1}}$, d_{pore} is the diameter of the pore considered as cylindrical.

The kinetic theory of gases (Bird et al., 2002) is used to calculate the dynamic viscosity of gas species, μ_i, and their mixture, μ. Finally the description is completed by the ideal gas law.

Table 3
Materials properties at 1173 K

Element	σ_s ($\Omega^{-1}\,m^{-1}$)	ε	κ (m^2)	λ_B ($W\,m^{-1}\,K^{-1}$)	A/V (m^{-1})	d_{pore} (m)	σ_M ($\Omega^{-1}\,m^{-1}$)
Anode Ni-YSZ	5	0.40	1×10^{-12}	6.23	2.2×10^6	1×10^{-6}	2.9×10^4
Cathode $LaMnO_3$-YSZ	5	0.40	1×10^{-12}	11	–	1×10^{-6}	1.02×10^4
Electrolyte YSZ	7	0.001	1×10^{-18}	2.7	–	1×10^{-6}	–

Table 4
Gas flows at the anode

x_{H_2O}/x_{CH_4}	Anodic flows ($kg\,s^{-1}$)
1	1×10^{-5}
0.1	$5,23\,529 \times 10^{-6}$
0.01	$4,75\,882 \times 10^{-6}$

3. Results and discussion

The high operating temperature of the SOFC allows operation in DIR and even in GIR. Both DIR and GIR enable the system to produce in situ the hydrogen required by the electrochemical reaction. However, unlike DIR, where the steam is fed in large amounts, the GIR process requires a very small quantity of steam since it uses the steam generated by the electrochemical reaction in the steam reforming reaction. Moreover, in DIR, because of the great difference between the reaction rates of the endothermic methane reforming reaction and the exothermic electrochemical hydrogen oxidation, cooling effects arise resulting in a temperature drop at the cell inlet (Aguiar et al., 2004). With operation in GIR, a delocalization of the steam reforming reaction along the cell may occur and, consequently, it would imply homogenization of the temperature gradient. Only an increase in cell temperature should be observed, because of the electrochemical reaction. However, at these working temperatures, Boudouard and cracking reactions can also be favoured. Carbon formation is consequently possible, with the risk of carbon deposits polluting the anode. A carbon deposit on the anode surface can obviously block the fuel supply and the transfer of the oxide ions, leading to a decrease in the power efficiency of the cell.

3.1. Electrochemical performances

A mixture of fuel and steam is injected at the anode side and air is fed at the cathode. The different x_{H_2O}/x_{CH_4} molar ratios are 0.01, 0.1 and 1 at the anode. The value of 0.1 is the arbitrary boundary between GIR and DIR. The value of 1 corresponds to the commonly allowed boundary beyond which carbon formation is unlikely (Klein et al., in press; Morel et al., 2005). The flows of these various mixtures are varied to keep a constant molar flow of methane in the cell, whatever the ratio used. These different flows are presented in Table 4.

The air flow at the cathode is sufficiently high ($10^{-3}\,kg\,s^{-1}$) to ensure that the molar fraction of oxygen at the cathode side varies only slightly. Such processing conditions were imposed to avoid limitations due to oxygen reduction at the cathode by a significant reduction in the oxygen concentration along the cell.

The polarization curves (Fig. 3) allow comparison of the electrochemical performance of the SOFC in GIR and DIR. It can be seen that performance of the cell is slightly higher for a low steam-to-methane ratio. Indeed, open circuit voltage is higher in GIR due to the low steam partial pressure at the anodic side. This result would seem to confirm that for a SOFC, a GIR process is very promising for thermodynamic reasons.

To explain these similarities in the iV curves, a thorough study of the simulation results, related to the hydrogen partial pressure and the reaction kinetics, is needed.

Fig. 4(a) and (b) presents, respectively, the reforming and shift reaction kinetics along the anode for operation in GIR and with $x_{H_2O}/x_{CH_4} = 0.1$. Fig. 4(c) and (d) presents the reforming and shift kinetics along the anode for operation in DIR with $x_{H_2O}/x_{CH_4} = 1$. A current density of $340\,mA\,cm^{-2}$ is imposed between the collectors.

The reforming kinetics (Fig. 4(a)) get slower along the cell because of the depletion of methane in the cell. The most significant kinetics gradient is localized on the first 10 mm of the cell. The kinetic rate then decreases much more slowly. Due to the low diffusion limitation, the kinetic rate is relatively homogeneous throughout the anode thickness. With regard to the kinetic rate of the water gas shift reaction (Fig. 4(b)), several phenomena can be noticed. First, the kinetic rates of the shift reaction are always positive, indicating that the equilibrium of this reaction moves towards more CO_2 and H_2 production rather than CO. This result is also found in the literature (Clarke et al., 1997). The increase in kinetic rates at the cell inlet is due to the fact that the system is not at equilibrium because hydrogen is not introduced adequately. The quantity of steam produced by the electrochemical reaction is thus sufficient to feed the reforming reaction throughout the cell. Moreover, the kinetics values are slightly higher close to the electrolyte–anode interface. Note that this interface is characterized by the value $r = 0$ whereas the contact area between the cermet and the gas channel is characterized by $r = 0.2$ mm. This result appears logical since most of the steam is produced close to the interface by the electrochemical reaction (Campanari and Iora, 2004; Matelli and Bazzo, 2005). Finally, the kinetics data show that the water gas shift reaction becomes really close to thermodynamic equilibrium (values ten times lower than for the reforming kinetics values: 1×10^{-3}–$1 \times 10^{-6}\,mol\,L^{-1}\,s^{-1}$).

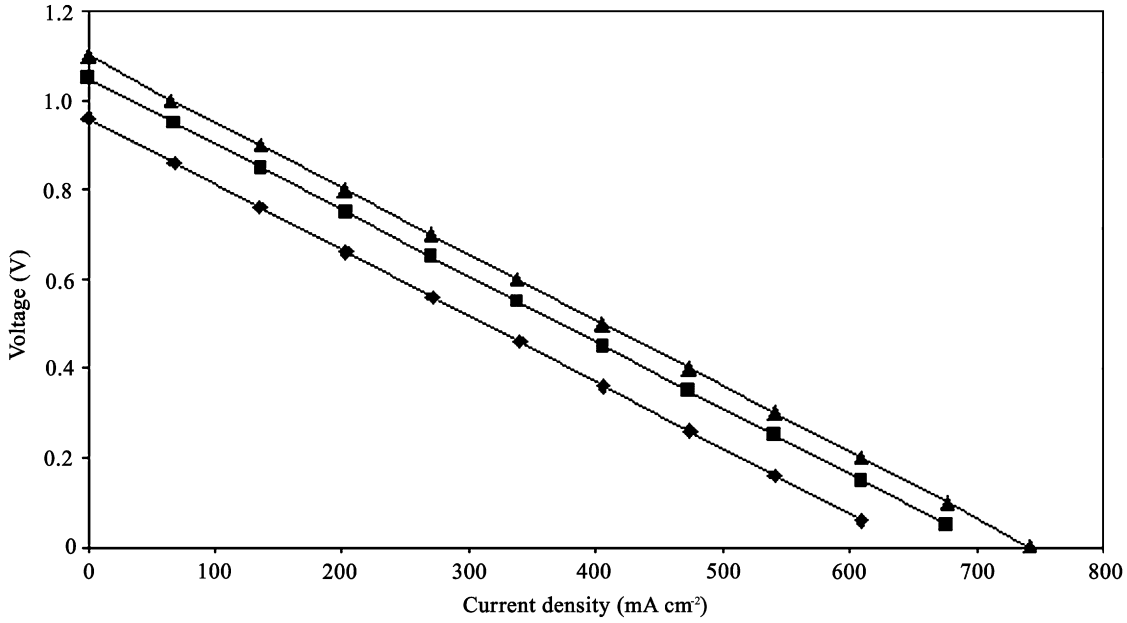

Fig. 3. Calculated polarization curves for various x_{H_2O}/x_{CH_4} ratios: ♦: $x_{H_2O}/x_{CH_4} = 1$; ■: $x_{H_2O}/x_{CH_4} = 0.1$; ▲: $x_{H_2O}/x_{CH_4} = 0.01$.

The shape of the reforming curve in DIR for a ratio $x_{H_2O}/x_{CH_4} = 1$ (Fig. 4(c)) is appreciably the same as that presented in Fig. 4(a). However, the steam reforming reaction is twice as fast at the cell inlet in DIR. This is due to the presence of a large quantity of steam fed into the anodic gas channel. Subsequently, there is a sharp decrease in the kinetic rate at the beginning of the cell, as confirmed by Aguiar et al. (2004). After 10 mm, kinetic rates are similar to those for GIR reforming. A much greater quantity of hydrogen is thus created at the inlet of the cell in DIR. Because of the high steam content at the inlet of the cell, the shift reaction is moved considerably towards the left (Fig. 4(d)). The water gas shift kinetic rates then stabilize.

To conclude this part, it can be said that the reforming kinetics decrease all along the cell. Slower changes are observed in GIR than in DIR because of the low steam content in the GIR injected gas. The water gas shift reaction is found to be close to equilibrium whatever the operating mode (GIR or DIR). However, in both modes, a slight displacement of the equilibrium towards the production of CO_2 and H_2 is observed.

Fig. 5 presents the distribution of hydrogen partial pressure along the anode for a ratio $x_{H_2O}/x_{CH_4}=0.1$. A zoom presenting this distribution according to the thickness is also given.

The hydrogen partial pressure, for a ratio $x_{H_2O}/x_{CH_4} = 0.1$ (Fig. 5), increases over the length of the cell considered. Since the electrochemical reaction taking place simultaneously, we can say that hydrogen is produced in sufficient amounts by the chemical reactions involved. The water gas shift reaction always being in a state very close to chemical equilibrium, hydrogen is produced almost exclusively by the steam reforming reaction. Fig. 5 also shows that two-thirds of the hydrogen are produced in the first 10 millimeter of the cell. The production rate then slows down considerably and the system moves towards equilibrium. This is in agreement with the reforming kinetics, which are very fast at the cell inlet and then tend towards chemical equilibrium. Finally, the zoom presented in Fig. 5 shows the hydrogen partial pressure as a function of the anode thickness. Since the catalytic reforming reaction takes place only within the anode, there is first an increase in the hydrogen partial pressure from the electrode–gas interface followed by a decrease, close to the electrolyte, due to electrochemical consumption.

To complete the description, the H_2O, CO, CH_4 and CO_2 partial pressure distributions are given in Fig. 6. First a decrease in the H_2O distribution can be observed due to the reforming reaction. Then an increase occurs because of the electrochemical reaction along the gas channel.

Fig. 7(a) and (b) compares the shape of the hydrogen partial pressures for ratios $x_{H_2O}/x_{CH_4}=0.01$ and $x_{H_2O}/x_{CH_4}=1$ (DIR).

The shape of the partial pressures is the same in GIR or DIR whatever the x_{H_2O}/x_{CH_4} ratio used. The quantity of hydrogen provided to the system by the reforming reaction is thus sufficient to feed the electrochemical reaction. At the same time, this implies that the quantity of steam provided by the electrochemical reaction is also sufficient to feed the reforming reaction. However, the x_{H_2O}/x_{CH_4} ratio used nevertheless has an influence on the system. First of all, the lower the x_{H_2O}/x_{CH_4} ratio, the smaller the quantity of hydrogen produced. In fact, the reforming reaction is faster in DIR than in GIR due to the quantity of steam injected in the cell. Thus it can be seen that the higher the x_{H_2O}/x_{CH_4} ratio, the faster the system reaches a homogeneous state (constant value of hydrogen partial pressure).

Finally, in terms of electrochemical performance, operation in GIR seems to be advantageous. Indeed, the minor modifications in operation described above do not have significant effects on the performance of the cell. Furthermore, operation in GIR tends to homogenize the partial pressures throughout the cell.

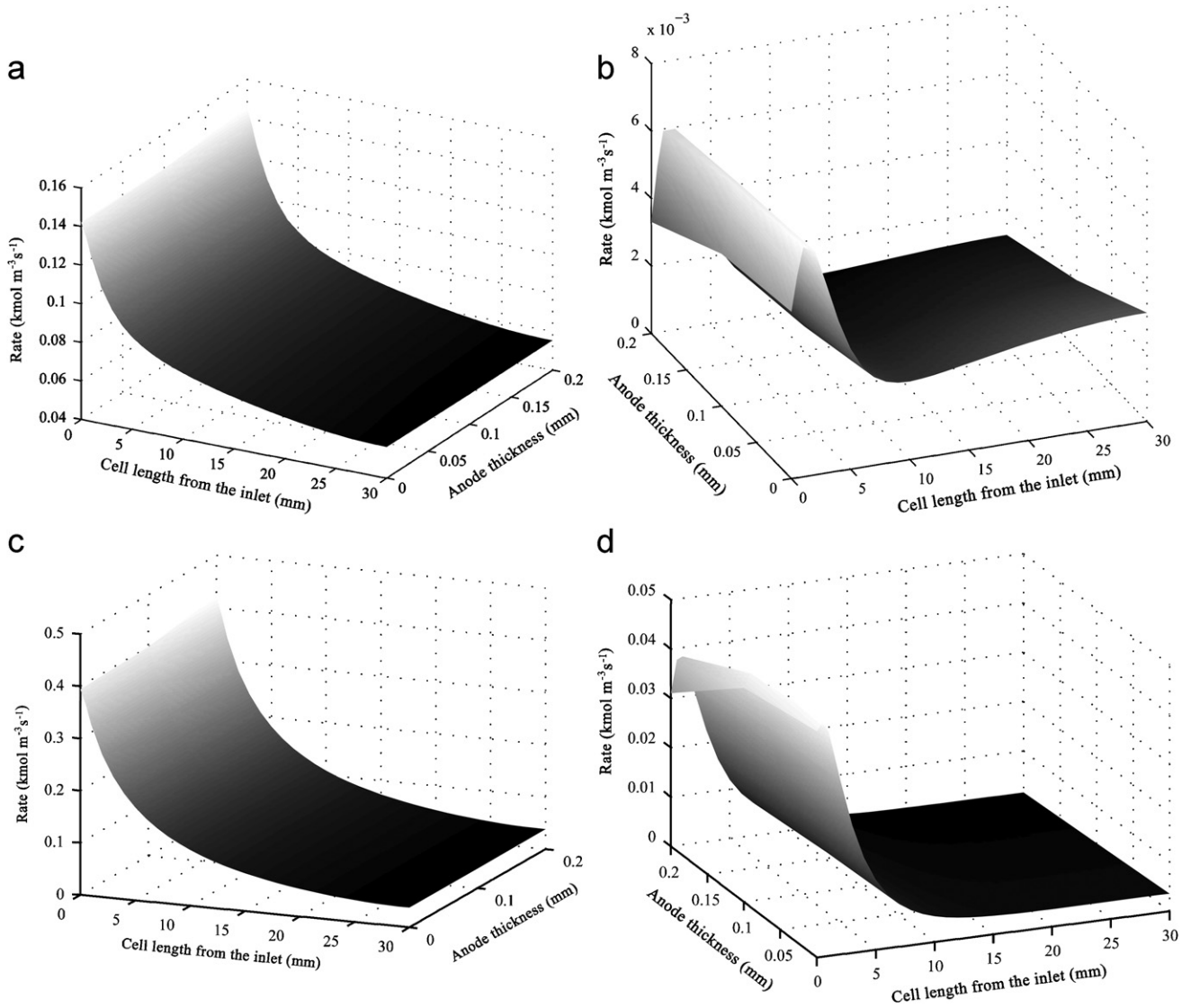

Fig. 4. (a) Reforming kinetics in GIR, (b) water gas shift kinetics in GIR; (c) reforming kinetics in DIR; (d) water gas shift kinetics in DIR.

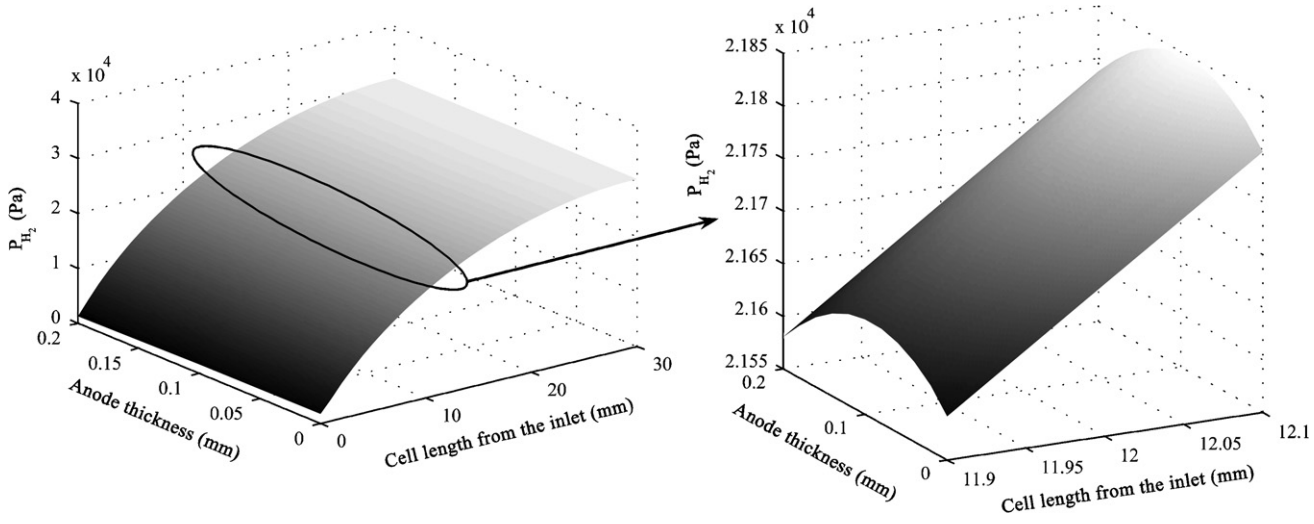

Fig. 5. Anodic hydrogen partial pressure in GIR.

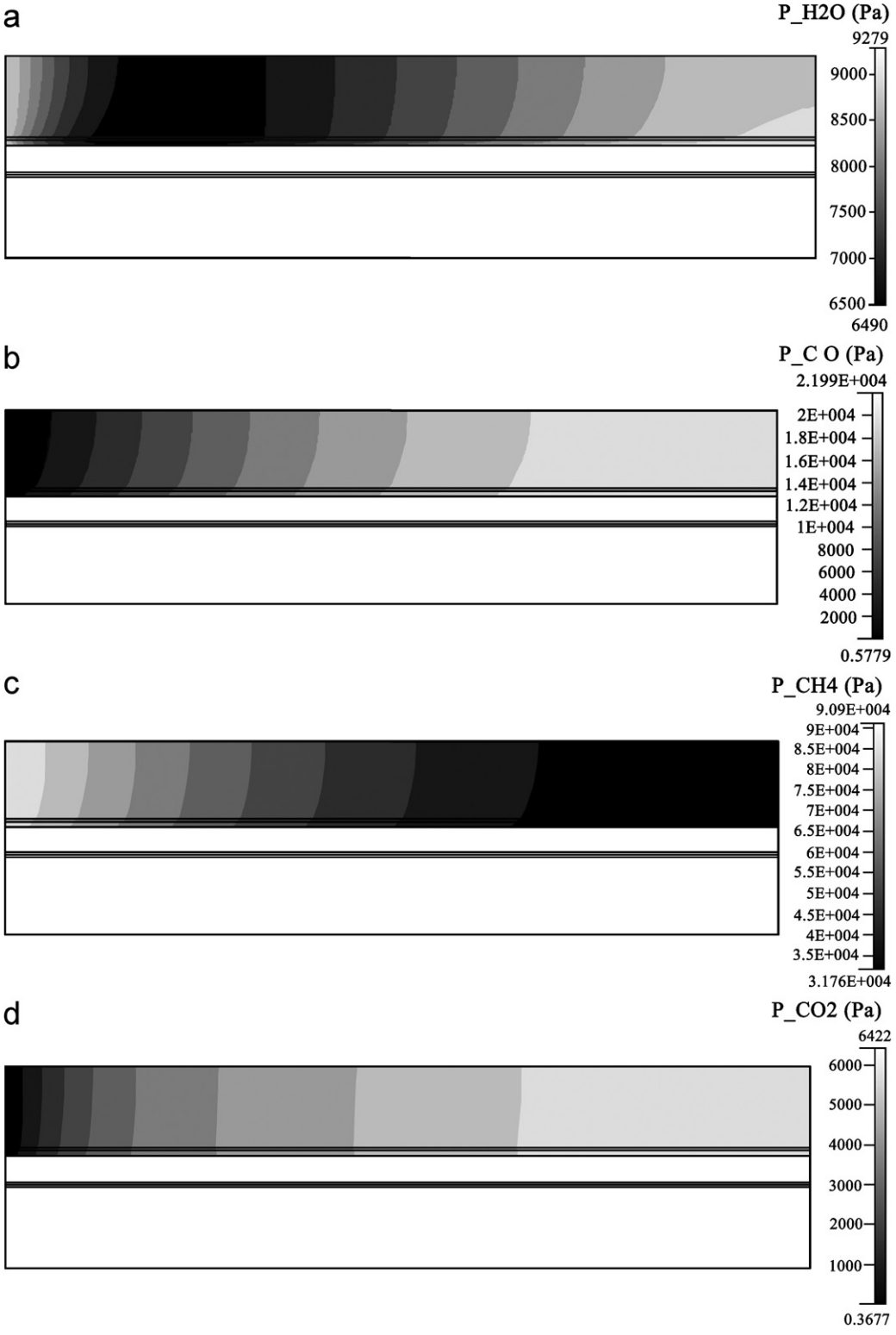

Fig. 6. (a) H_2O partial pressure (Pa); (b) CO partial pressure (Pa); (c) CH_4 partial pressure (Pa); (d) CO_2 partial pressure (Pa).

3.2. Thermal behaviour of the cell in GIR and DIR

Fig. 8(a) and (b) presents, respectively, the temperature variations at the anodic side of the cell in DIR and GIR. It is important to remember that only the inlet and the first three centimetres of the cell are modelled. In DIR (Fig. 8(a)), a cooling effect in the first centimetre of the cell can be observed because of the big difference between the reaction rates of the endothermic methane reforming reaction and exothermic electrochemical hydrogen oxidation (Aguiar et al., 2004). The

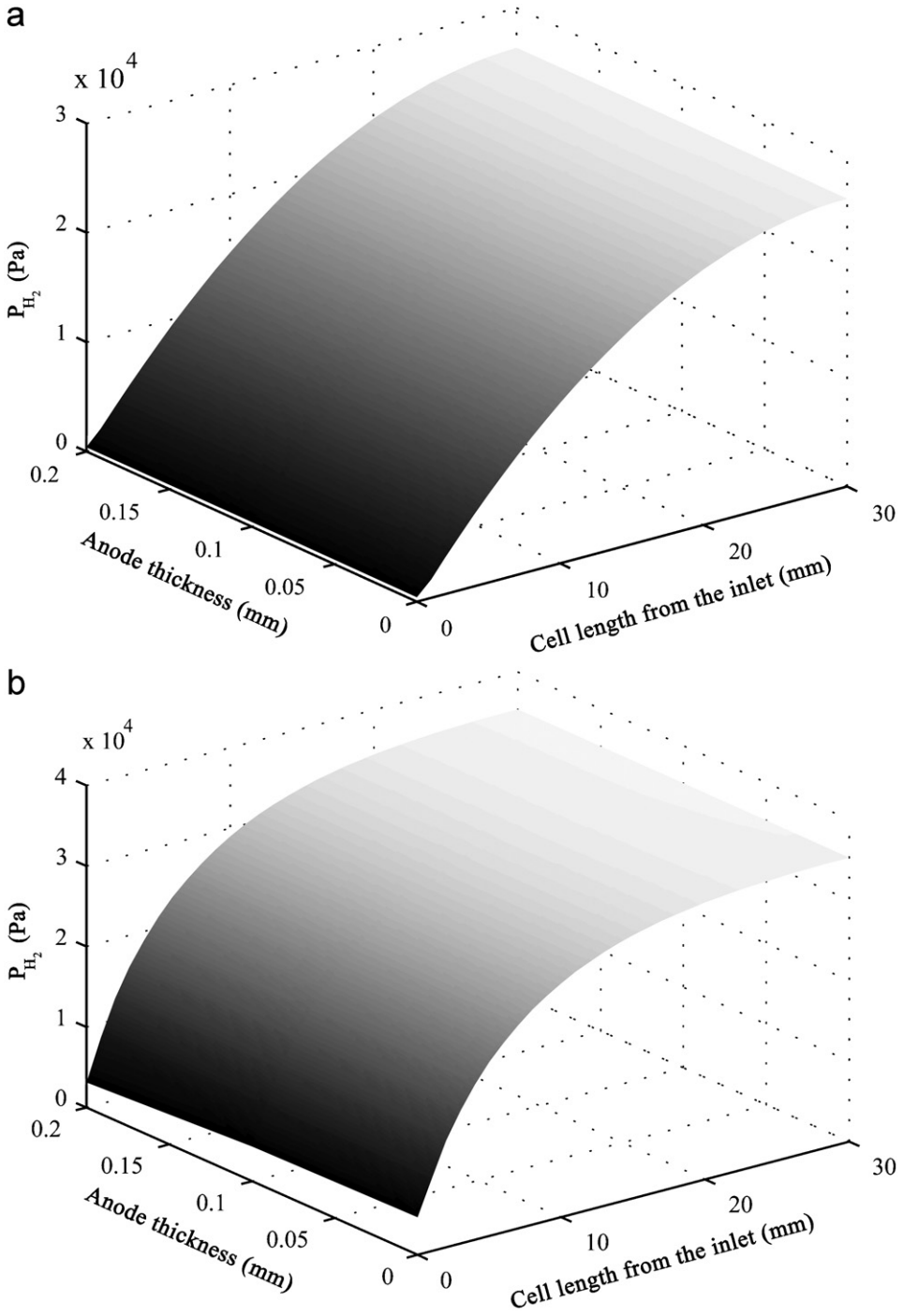

Fig. 7. (a) Hydrogen partial pressure for $x_{H_2O}/x_{CH_4} = 0.01$; (b) hydrogen partial pressure for $x_{H_2O}/x_{CH_4} = 1$.

temperature increase due to exothermic hydrogen oxidation can also be observed. Indeed the reaction rate of the exothermic reaction becomes faster than that of the endothermic reaction.

Temperature behaviour is completely different in GIR (Fig. 8(b)) because of the delocalization of the reforming reaction and the disappearance of the cooling effect. The exothermic oxidation rate is slightly higher than the reforming reaction rate and so only a temperature increase can be observed. It should be added that the temperature increase is not as great as it would be if operation with pure hydrogen were used. This is one of the major interests of the GIR method with regard to mechanical stress.

3.3. Problems involved in relation to carbon deposition

Carbon formation is a serious problem in SOFCs that involve methane at high temperatures in both GIR and DIR.

At the anode side, the conversion process includes steam methane reforming (Eq. (4)) associated with shift (Eq. (5)) and electrochemical (Eq. (6)) reactions, but also the para-

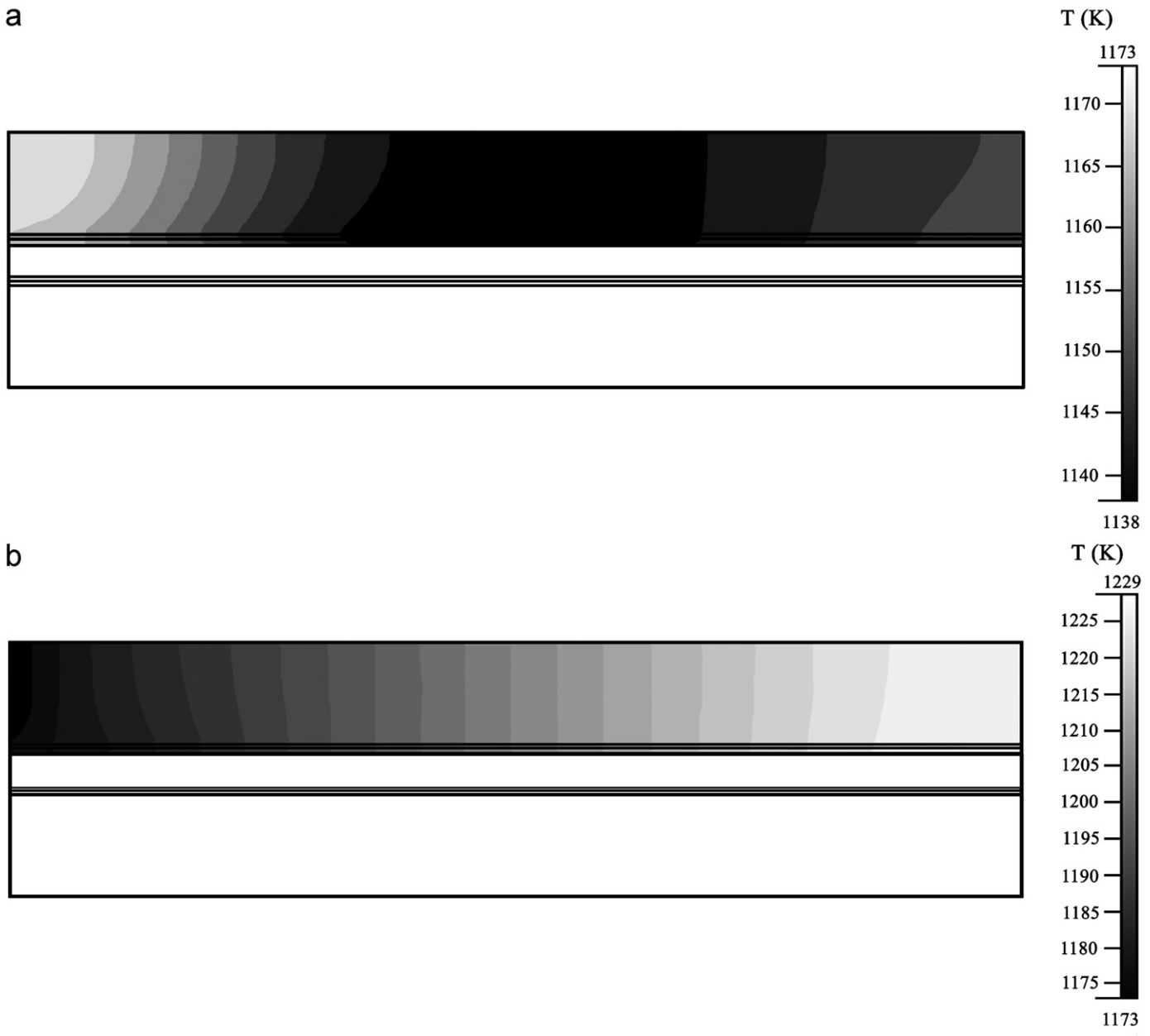

Fig. 8. (a) Temperature gradient in the cell in DIR; (b) temperature gradient in the cell in GIR.

sitic Boudouard and cracking reactions which can lead to the formation of a carbon deposit.

Therefore, a detailed thermodynamic analysis is necessary to predict the carbon formation boundary for SOFCs fuelled by methane. The Boudouard reaction and the cracking reaction are the major pathways for carbon formation at high operating temperatures (Amor, 1999).

The reactional quotient of these two reactions can be written (Eqs. (15), (16)):

$$Q_B = \frac{P_{CO_2} \times a_c}{P_{CO}^2}, \tag{15}$$

$$Q_C = \frac{P_{H_2}^2 \times a_c}{P_{CH_4}}, \tag{16}$$

where Q_B and Q_C are, respectively, the reactional quotients of the Boudouard and cracking reactions. a_c represents carbon activity and will be taken equal to 1 in calculations. Finally P_i is the partial pressure of various gas species i.

The results will be discussed from the values of driving forces for carbon deposition, defined as the ratios α and β depending on the respective reactional quotients and on the equilibrium constants K_B and K_C of the Boudouard and cracking reactions (Hou and Hughes, 2001; Sangtongkitcharoen et al., 2005)

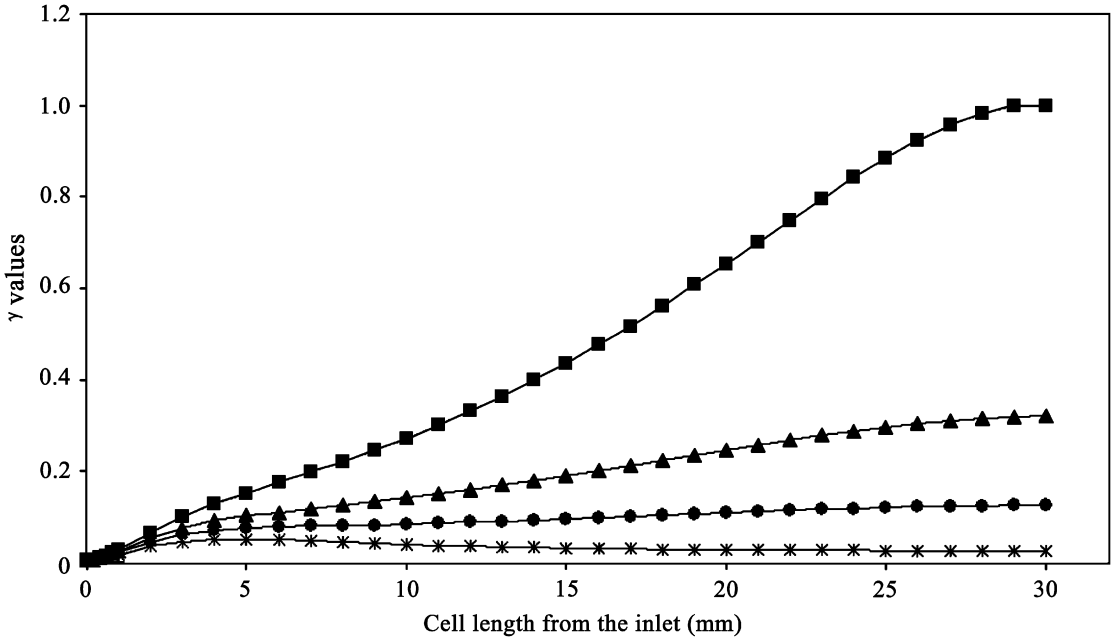

Fig. 9. γ Coefficient profiles along the length of the cell from the inlet for different current densities and for a x_{H_2O}/x_{CH_4} ratio of 0.1: ■: 609 mA cm^{-2}; ▲: 338 mA cm^{-2}; ●: 203 mA cm^{-2}; ✱: 67.6 mA cm^{-2}.

which are temperature functions

$$\alpha = \frac{Q_B}{K_B} = \frac{P_{CO_2} a_c}{P_{CO}^2 K_B}, \tag{17}$$

$$\beta = \frac{Q_C}{K_C} = \frac{P_{H_2}^2 a_c}{P_{CH_4} K_C}. \tag{18}$$

For each reaction, if α or $\beta < 1$, the system is not at equilibrium and the reaction will proceed towards the right. In this case carbon deposition is thermodynamically favoured. Equilibrium is reached when α or $\beta = 1$. On the other hand, for α or $\beta > 1$, carbon formation is thermodynamically impossible and the reaction will proceed towards the left.

This phenomenon would take place in the area where carbon deposition is thermodynamically favoured. The local values of parameters α and β are then calculated from the distributions of partial pressures within the two-dimensional porous anode. Finally, their mapping enables us to predict the predominance zones where carbon formation is favoured or prevented according to thermodynamics.

As demonstrated by a previous thermodynamic study presented in Klein et al. (in press), of the two reactions where carbon is present, only the cracking reaction proceeds to the right and could yield carbon. In the case of the Boudouard reaction, the trend is to proceed toward the left. This observation indicates that to some extent the Boudouard reaction may play a role in decoking. After these preliminary considerations, it would appear of great interest to investigate the simultaneous influences of both reactions through the coefficient γ (Eq. (19))

$$\gamma = \alpha \times \beta. \tag{19}$$

It has been demonstrated that the risk of carbon formation is higher when the steam-to-methane ratio is decreased.

However, further studies are needed, in particular because the carbon formation rate has not yet been taken into account and therefore there is still no information available concerning the rate of anode pollution.

Finally, Fig. 9 presents the γ (Eq. (19)) distribution along different lengths of the fuel cell from the inlet for several current densities (609, 338, 203, 67.6 mA cm^{-2}) and for a x_{H_2O}/x_{CH_4} ratio of 0.1.

It can be observed that the lower the current density, the smaller the value of γ. Indeed, with a low current density, the kinetics of the electrochemical reaction are not very fast. So there is steam depletion and thus a greater tendency to cracking. Finally, it can be seen that for low current densities, the γ parameter does not change much throughout the cell. Thus, for high current densities, carbon deposition is thermodynamically more favoured at the cell inlet whereas for low current densities carbon formation is favoured on the entire cell.

To conclude, it can be said that the problem of carbon deposition is exacerbated during GIR operation. Moreover, with low current densities, it is likely to occur on the entire cell and in considerable proportions.

4. Conclusion

A model using the CFD-Ace software package has been developed for gradual internal reforming (GIR) at the anode of a tubular SOFC. The model is compared with a tubular SOFC operating in DIR.

Simulation allows the prediction of gas partial pressures distributions (CH_4, H_2, CO, CO_2, H_2O), temperature distribution in the cell, current density and the potentials of the electronic and ionic phases within the anode part (i.e., gas channel and cermet anode). As expected, the steam reforming reaction of CH_4 should largely occur within the electrode part close to the gas inlet, then lead to a sharp increase in the hydrogen partial pressure with operation in DIR. In GIR, homogenization of the steam reforming kinetics can be observed. However, in GIR, as in DIR, the quantity of hydrogen produced is higher than the quantity of hydrogen required by the electrochemical reaction. As a consequence, the electrochemical performance of the cell is similar in GIR and DIR.

Furthermore, the temperature distributions have been calculated in the cell in GIR and DIR. The main result is that the cooling effect due to the endothermic reforming reaction disappears in GIR mode.

Moreover, a detailed thermodynamic analysis based on three characteristic parameters α, β and γ has been carried out to predict the boundary for carbon formation in a SOFC due to methane cracking and Boudouard reactions. By mapping the α, β and γ values we were able to predict that there is a significant tendency for methane cracking, which could result in carbon formation. However, the reverse Boudouard reaction seems to be favourable, since it could form CO from the deposited carbon, leading to possible decoking. The γ values are indicators for assessing the contributions of both reactions in the system. On the basis of the γ values, carbon formation can be assumed for x_{H_2O}/x_{CH_4} ratios lower than one. In GIR, carbon formation can therefore be a serious problem. To alleviate this problem, both the cell geometry and the catalyst dispersion must be adjusted in order to optimize the specific catalytic area. A catalyst layer where carbon deposition is not favoured can be added at the surface of the anode. Most of the fuel will be reformed in this catalytic area and so the problem of coking should be significantly reduced.

Notation

a_c	carbon activity, dimensionless
d_{pore}	pore diameter, m
D_i	diffusion coefficient of the ith species, $m^2\,s^{-1}$
$D_{i,\text{eff}}$	effective diffusion coefficient of the ith species, $m^2\,s^{-1}$
E_0	voltage between the electrolyte and the nickel at equilibrium, V
F	Faraday constant (96 500), $c\,mol^{-1}$
h	gas mixture enthalpy, $J\,kg^{-1}$
h_i	enthalpy of the ith species, $J\,kg^{-1}$
h_B	solid phase enthalpy, $J\,kg^{-1}$
$[i]$	molar concentration of the ith species, $kmol\,m^{-3}$
$[i]_0$	reference concentration of the ith species, $kmol\,m^{-3}$
j_{a0}	exchange current density of the anode, $A\,m^{-2}$
j_{at}	Faradic current due to anodic reaction, $A\,m^{-2}$
j_{ct}	Faradic current due to cathodic reaction, $A\,m^{-2}$
J_i	diffusion flux of the ith species, $mol\,m^{-2}\,s^{-1}$
K_B	equilibrium constant of Boudouard reaction, Pa^{-1}
K_C	equilibrium constant of Cracking reaction, Pa
M	molecular weight of the mixture of gases, $kg\,kmol^{-1}$
p	total pressure, Pa
P_i	partial pressure of the ith species, Pa
q	heat flux, $W\,m^{-2}$
r_k	reaction rate of the kth reaction, $kmol\,m^{-3}\,s^{-1}$
R	universal gas constant (8314), $J\,mol^{-1}\,K^{-1}$
$(S/V)_{\text{eff}}$	effective surface-to-volume ratio, $m^2\,m^{-3}$
T	temperature, K
v	fluid velocity, $m\,s^{-1}$
w_i	mass fraction of the ith species, dimensionless
x_i	molar fraction of the ith species, dimensionless

Greek letters

α	Boudouard coefficient, dimensionless
α_a	anodic Tafel constant, dimensionless
α_c	cathodic Tafel constant, dimensionless
β	cracking coefficient, dimensionless
γ	Boudouard + cracking coefficient, dimensionless
δ	shear stress tensor, dimensionless
ε	porosity, dimensionless
η_a	anode overpotential, V
κ	permeability, m^2
λ	thermal conductivity of the porous medium, $W\,m^{-1}\,K^{-1}$
λ_B	thermal conductivity of the solid phase, $W\,m^{-1}\,K^{-1}$
λ_F	thermal conductivity of the fluid phase, $W\,m^{-1}\,K^{-1}$
μ	dynamic viscosity of the gas mixture, Pa s
μ_i	dynamic viscosity of the ith species, Pa s
ρ	mass density of the gas mixture, $kg\,m^{-3}$
ρ_B	mass density of the solid phase, $kg\,m^{-3}$
σ_{aS}	ionic phase conductivity at anode, $\Omega^{-1}\,m^{-1}$
σ_{aM}	electronic phase conductivity at anode, $\Omega^{-1}\,m^{-1}$
σ_{eS}	ionic phase conductivity of the electrolyte, $\Omega^{-1}\,m^{-1}$
τ	tortuosity of pores, $m\,m^{-1}$
ϕ_{aS}	ionic phase potential at anode, V
ϕ_{aM}	electronic phase potential at anode, V
ϕ_{eS}	ionic phase potential of the electrolyte, V

Acknowledgments

The authors extend their warmest thanks to Prof. J. Fouletier, Dr J. Deseure and M. Henault for many fruitful discussions.

References

Ackmann, T., de Haart, L.G.J., Lehnert, W., Stolten, D., 2003. Modeling of mass and heat transport in planar substrate type SOFCs. Journal of the Electrochemical Society 150 (6), A783–A789.

Aguiar, P., Adjiman, C.S., Brandon, N.P., 2004. Anode-supported intermediate temperature direct internal reforming solid oxide fuel cell. I: model-based steady-state performance. Journal of Power Sources 132, 113–126.

Ahmed, K., Foger, K., 2000. Kinetics of internal steam reforming of methane on Ni/YSZ based anodes for solid oxide fuel cells. Catalysis Today 63, 479–487.

Amor, J.N., 1999. The multiple roles for catalysis in the production of H_2. Apply Catalysis A 176, 159–176.

Aruna, S.T., Muthuraman, M., Patil, K.C., 1998. Synthesis and properties of Ni-YSZ cermet: anode material for solid oxide fuel cells. Solid State Ionics 111, 45–51.

Bird, R.B., Byron, R., Stewart, W.E., Lightfoot, E.N., 1960. Transport Phenomena. Wiley, New York.

Bird, R.B., Byron, R., Stewart, W.E., Lightfoot, E.N., 2002. Transport Phenomena, second ed. Wiley, New York.

Bruggemann, D.A.G., 1935. Annalen der Physik (Leipzig) 24, 636.

Campanari, S., Iora, P., 2004. Definition and sensitivity analysis of a finite volume SOFC model for a tubular cell geometry. Journal of Power Sources 132, 113–126.

Clarke, S.H., Divks, A.L., Pointon, K., Smith, T.A., Swann, A., 1997. Catalytic aspects of the steam reforming of hydrocarbons in internal reforming fuel cells. Catalysis Today 38, 411–423.

Costamagna, P., Panizza, M., Cerisola, G., Barbucci, A., 2002. Effect of composition on the performance of cermet electrodes. Experimental and Theoretical Approach. Electrochimica Acta 47, 1079–1089.

EG&G Services, 2000. Fuel Cell Handbook, fifth ed. Science Applications International Corporation, US Department of Energy, pp. 8–5.

ESI group, 2006. CFD-Ace + V2006, Manuals.

Fontes, E., Lagergren, C., Simonsson, D., 1997. Mathematical modelling of the MCFC cathode on the linear polarisation of the NiO cathode. Journal of Electroanalytical Chemistry 432, 121–128.

Georges, S., Parrour, G., Henault, M., Fouletier, J., 2006. Gradual internal reforming of methane: a demonstration. Solid State Ionics 177, 2109–2112.

Hecht, E.S., Gupta, G.K., Zhu, H., Dean, A.M., Kee, R.J., Maier, L., Deutschmann, O., 2005. Methane reforming kinetics within a Ni-YSZ SOFC anode support. Applied Catalysis 295, 40–51.

Hou, K., Hughes, R., 2001. The kinetics of methane steam reforming over a $Ni/\alpha - Al_2O$ catalyst. Chemical Engineering Journal 82, 311–328.

Klein, J.-M., Bultel, Y., Pons, M., Ozil, P., Modeling of a SOFC fuelled by methane: analysis of carbon deposition. Journal of Fuel Cell Science and Technology, in press.

Larrain, D., Van Herle, J., Maréchal, F., Favrat, D., 2003. Thermal modeling of a small anode supported solid oxide fuel cell. Journal of Power Sources 118, 367–374.

Lee, J.H., Moon, H., Lee, H.W., Kim, J., Kim, J.D., Yoon, K.H., 2002. Quantitative analysis of microstructure and its related electrical property of SOFC anode, Ni-YSZ cermet. Solid State Ionics 148, 15–26.

Lehnert, W., Meusinger, J., Thom, F., 2000. Modelling of gas transport phenomena in SOFC anodes. Journal of Power Sources 87, 57–63.

Li, P.W., Suzuki, K., 2004. Numerical modeling and performance study of a tubular SOFC. Journal of the Electrochemical Society 151 (4), A548–A557.

Matelli, J.A., Bazzo, E., 2005. A methodology for thermodynamic simulation of high temperature, internal reforming fuel cell systems. Journal of Power Sources 142, 160–168.

Mazumder, S., Cole, J.V., 2003. Rigorous 3-D mathematical modeling of PEM fuel cells. I. Model predictions with liquid water transport. Journal of the Electrochemical Society 150 (1), A1503–A1509.

Morel, B., Laurencin, J., Bultel, Y., Lefebvre-Joud, F., 2005. Anode-supported SOFC model centered on the direct internal reforming. Journal of the Electrochemical Society 152 (7), A1382–A1389.

Natarajan, D., Nguyen, T.V., 2001. A two-dimensional, two-phase, multicomponent, transient model for the cathode of a proton exchange membrane fuel cell using conventional gas distributors. Journal of the Electrochemical Society 148 (12), A1324–A1335.

Prins-Jansen, J.A., Fehribach, J.D., Hemmes, K., De Wit, J.H.W., 1996. A three-phase homogeneous model for porous electrodes in molten-carbonate fuel cells. Journal of the Electrochemical Society 143 (5), 1617–1628.

Sangtongkitcharoen, W., Assabumrungrat, S., Pavarajarn, V., Laosiripojana, N., Praserthdam, P., 2005. Comparison of carbon formation boundary in different modes of solid oxide fuel cells fuelled by methane. Journal of Power Sources 142, 75–80.

Springer, T.E., Zawodinski, T.A., Gottesfeld, S., 1991. Polymer electrolyte fuel cell model. Journal of the Electrochemical Society 138 (8), 2334–2342.

Suwanwarangkul, R., Croiset, E., Fowler, M.W., Douglas, P.L., Entchev, E., Douglas, M.A., 2003. Performance comparison of Fick's, dusty-gas and Stefan–Maxwell models to predict the concentration overpotential of a SOFC anode. Journal of Power Sources 122, 9–18.

Ullmann, H., Trofimenko, N., Tietz, F., Stöver, D., Ahmad-Khanlou, A., 2000. Correlation between thermal expansion and solid ion transport in mixed perovskite-type oxides for SOFC cathodes. Solid State Ionics 138, 79–90.

Vernoux, P., Guindet, J., Kleitz, M., 1998. Gradual internal methane reforming in intermediate-temperature solid-oxide fuel cells. Journal of the Electrochemical Society 145 (10), 3487–3492.

Vernoux, P., Guillodo, M., Fouletier, J., Hammou, A., 2000. Alternative anode material for gradual methane reforming in solid oxide fuel cell. Solid State Ionics 135, 425–431.

Yuh, C.Y., Selman, J.R., 1992. Porous-electrode modeling of the molten-carbonate fuel-cell electrodes. Journal of the Electrochemical Society 139 (5), 1373–1379.